A Tension-based Position Estimation Approach for Moored Marine Vessels

Zhengru Ren * **Roger Skjetne** * **Øivind Kåre Kjerstad** *

* *Department of Marine Technology, Norwegian University of Science and Technology, NO 7491 Trondheim, Norway, (e-mail: zhengrur@stud.ntnu.no, {roger.skjetne, oivind.k.kjerstad}@ntnu.no)*

Abstract: This paper presents a novel idea on a tension-based localization approach as a redundancy measure to handle the situation when the position reference (posref) signals are not available or significant GNSS drifts occur, such as sudden ionospheric disturbances, for thruster-assisted moored vessels. The only information needed is the tension measurements from tension cells. This method can improve the redundancy and safety of offshore operation, by detecting and verifying posref failure modes. It can even take over the posref function if one no longer trust the main posref measurements. Based on a residual signal, a fault detection and estimation approach is introduced and verified through simulations.

Keywords: Thruster-assisted position mooring; Position mooring; Position reference systems; Fault diagnosis.

1 Introduction

Commercially available from the 1980s, thruster-assisted position mooring (TAPM) is an important offshore stationkeeping method for floating structures with an energy-efficient feature. The main difference between a TAPM and a dynamic positioning (DP) is that, while a DP system uses the thrusters directly to control the position and heading, a TAPM system uses the thrusters only to assist the mooring lines in keeping the heading in a favorable direction with respect to the environmental loads, and adding surge/sway damping (Skjetne et al., 2014). The position itself is allowed to move within an acceptable region. Innovative industrial tension units, such as the INTEGRIpod^{TM} and the Inter-MPulse^{TM}, are used to monitor and detect the line breakage through tension measurements (Gauthier et al., 2014). Fault detection and isolation (FDI), and reconfiguration control (RC) are two main categories in fault-tolerant control (FTC) (Blanke et al., 2006). Research on FTC schemes to TAPM systems is, for example, presented by Fang and Blanke (2011), Fang et al. (2015), and Nguyen and Blanke (2015).

The global navigation satellite system (GNSS) provides the Earth-fixed position information to surface-based motion systems. GPS, being the most widely used, has been a necessary part to navigation systems of modern marine systems in recent decades. The differential global positioning systems (DGPS) improves the positioning accuracy. However, the GPS signals may experience drifts during some extreme conditions, such as solar events and sudden ionospheric disturbances (SID). SID is a phenomenon with sudden increase of electron density in the ionosphere caused by solar flares, earthquake, storm, or tsunami. It results in a sudden decrease of the upper medium frequency and lower high frequency components in radiowaves (Afraimovich et al., 2000). Normally, SID happens simultaneously with ionospheric storms. These phenomena can last for 1-3 days, even 10 days, significantly degrading the reliability of marine control systems (Tsugawa et al., 2011).

A typical posref drift failure mode in a DP system is that all GPS measurements starts to drift due to SID (Zhao et al., 2012). The hydroacoustic position reference (HPR) system does not drift, but due to the superior signal quality of the GPS signals over the HPR signals, the DP control system chooses to believe in the GPS signals and automatically disables the HPR measurement, thus making the situation worse with a resulting DP system drive-off.

Considering the long-term duration of TAPM stationkeeping operations, the probability of experiencing such drift events is high. Doherty et al. (2004) reported that three very large sunspot clusters happened in October-November 2003 which caused strong magnetic storms. A Large amount of satellites failed, jeopardising the safety of the operations.

This paper proposes a localization algorithm based on the mooring line tension measurement. This provides extra detection capability of posref failure modes and a redundant position reference. Treated as a backup solution in abnormal conditions, this tension-based localization method can improve redundancy with only software updates. It is a companion paper to Ren et al. (2015), which considers the problem of efficient linebreak detection in the case when tension sensors are not available in the TAPM system. Here we consider the converse case when tension sensors are available and can be used as redundancy to the posref systems.

2 Problem Formulation

2.1 Vessel model

A surface vessel is moored by M mooring lines and is equipped with thrust assist. All the cables are indexed with an integer $i \in \mathcal{I}$ where $\mathcal{I} = \{1, 2, \cdots, M\}$ is an index set. Each cable is connected to the turret at a specific fairlead. The distance between the fairlead and the center of turret (COT) is r_t. The turret can rotate about a vertical axis at the COT (see Fig. 1). The vessel is considered to keep its position in 3DOF, including surge, sway, and yaw. The environmental loads are wind, waves, and currents.

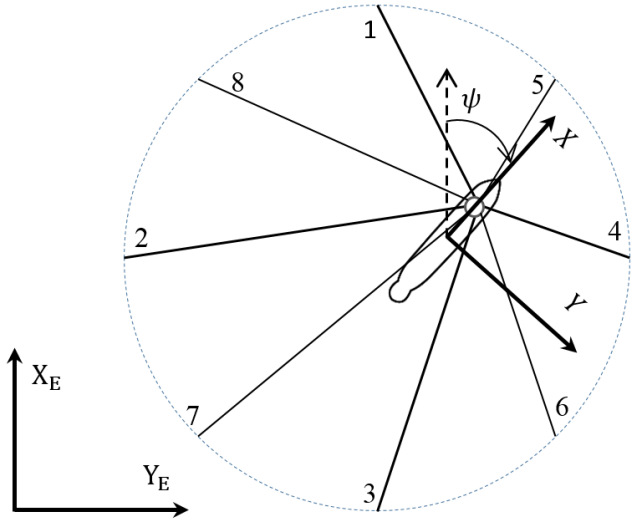

Fig. 1. System in Earth-fixed reference frame.

In what follows, the vessel model described in Fossen (2011) is presented. The stationkeeping model is given by

$$\dot{\boldsymbol{\eta}} = \boldsymbol{R}(\boldsymbol{\psi})\boldsymbol{\nu}, \tag{1a}$$

$$\boldsymbol{M}\dot{\boldsymbol{\nu}} + \boldsymbol{D}\boldsymbol{\nu} = \boldsymbol{R}(\psi)^{\top}\boldsymbol{b} + \boldsymbol{\tau_c} + \boldsymbol{\tau_m}, \tag{1b}$$

$$\dot{\boldsymbol{b}} = \boldsymbol{0}, \tag{1c}$$

where $\boldsymbol{\eta} = [x\ y\ \psi]^{\top}$ consists of the low frequency (LF) Earth-fixed position and heading orientation of the vessel relative to an Earth-fixed frame, $\boldsymbol{\nu} = [u\ v\ r]^{\top}$ represents the linear and rotational velocities decomposed in a vessel-fixed reference, $\boldsymbol{R}(\psi) \in \mathbb{R}^{3\times3}$ denotes the transformation matrix between the body-fixed frame and Earth-fixed frame(see Fig. 1), $\boldsymbol{M} \in \mathbb{R}^{3\times3}$ is the generalized system inertia matrix including zero frequency added mass components, $\boldsymbol{D} \in \mathbb{R}^{3\times3}$ denotes the linear damping matrix, $\boldsymbol{b} \in \mathbb{R}^3$ is a slow varying bias vector in the earth frame, $\boldsymbol{\tau_c} \in \mathbb{R}^3$ represents thruster induced forces vector, and $\boldsymbol{\tau_m} \in \mathbb{R}^3$ is the mooring load vector. See Fossen (2011) and Sørensen (2012) for details.

2.2 Mooring forces

The mooring system is modeled statically by catenary equations, disregarding the cable dynamics, the higher mode full-profile motion, nonlinear damping, and vibrations. For the LF model, a horizontal-plane spread mooring model is formulated as

$$\boldsymbol{\tau_m} = -\boldsymbol{R}(\psi)^{\top}\boldsymbol{g}_{mo}(\boldsymbol{\eta}) - \boldsymbol{d}_{mo}(\boldsymbol{\nu}), \tag{2}$$

where it is assumed that the mooring system is symmetrically arranged. Assuming fixed anchor line length, the damping effects of the mooring lines can be approximated by a linear damping model $\boldsymbol{D}_{mo}\boldsymbol{\nu}$. It is a common practice to estimate the linear damping of the mooring line by about $10-20\%$ of critical damping of the entire system (Nguyen et al., 2011). We have augmented the linear damping of the mooring system into the damping term $\boldsymbol{D\nu}$. The Earth-fixed restoring force $\boldsymbol{g_{mo}}(\boldsymbol{\eta}) \in \mathbb{R}^3$ is given by

$$\boldsymbol{g}_{mo}(\boldsymbol{\eta}) = \boldsymbol{T}(\boldsymbol{\beta})\boldsymbol{\tau}_H, \tag{3}$$

where $\boldsymbol{\beta} \in \mathbb{R}^M$ is the mooring line orientation vector consisting of the angles between the mooring lines and the x-axis, $\boldsymbol{\tau}_H = [H_1, H_2, \cdots, H_M]^{\top}$ denotes the horizontal mooring force vector, and H_i represents the horizontal force component at TP_i. Suppose the moment provided by the mooring restoring forces is disregarded, the mooring line configuration matrix is

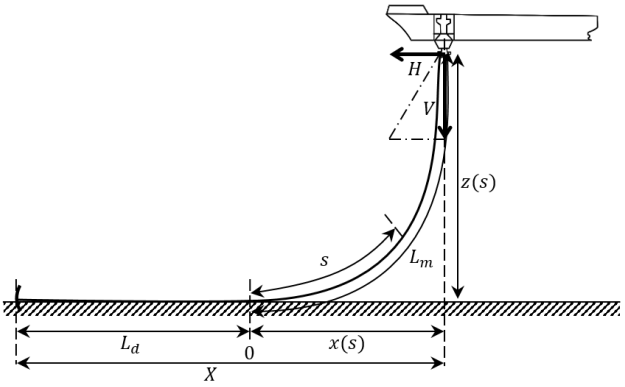

Fig. 2. Mooring line configuration.

$$\boldsymbol{T}(\boldsymbol{\beta}) = \begin{bmatrix} cos\beta_1 & \cdots & cos\beta_M \\ sin\beta_1 & \cdots & sin\beta_M \\ 0 & \cdots & 0 \end{bmatrix}. \tag{4}$$

Fig. 2 shows the configuration of a single mooring line. The 2D catenary equations (5a) and (5b) are used in this case to calculate H_i and the vertical mooring force component V_i (Aamo and Fossen, 2001).

$$x_i(s) = \frac{H_i}{E_m A_m}s + \frac{H_i}{\omega_m}\left\{ sinh^{-1}\left[\frac{V_i - \omega_m\left(L_m - s\right)}{H_i}\right] - sinh^{-1}\left[\frac{V_i - \omega_m L_m}{H_i}\right]\right\}, \tag{5a}$$

$$z_i(s) = \frac{1}{E_m A_m}\left[V_i s + \frac{\omega_m}{2}\left(\left(L_m - s\right)^2 - L_m^2\right)\right] + \frac{H_i}{\omega_m}\left[\sqrt{1+\left(\frac{V_i - \omega_m\left(L_m - s\right)}{H_i}\right)^2} + \sqrt{1+\left(\frac{V_i - \omega_m L_m}{H_i}\right)^2}\right], \tag{5b}$$

where s is the path parameter along the cable, $x_i(s)$ and $z_i(s)$ are the positions of each segment centred at length s along the i^{th} cable, L_m is the unstretched suspended segment length of the mooring lines, ω_m is the weight in water per unit length, E_m is the Young's modulus of elasticity, A_m stands for the cross-section area of the line, $T_i = \sqrt{V_i^2 + H_i^2}$ is tension at the end of the i^{th} mooring line, and $\phi_i = arctan(V_i/H_i)$ is the angle between the line tension and its vertical component. When the attachment point moves in either the horizontal plane or the vertical plane, L_m and the touchdown length L_d vary. The unstretched length of the mooring lines is supposed to be a constant, such that $L = L_d + L_m$.

2.3 Control law

The corresponding PID controller for thrust assist is designed to keep the LF heading and position at desired values. The PID controller is given by

$$\dot{\boldsymbol{\xi}} = \tilde{\boldsymbol{\eta}}, \tag{6a}$$

$$\boldsymbol{\tau}_c = -\boldsymbol{K}_i\boldsymbol{R}(\psi)^{\top}\boldsymbol{\xi} - \boldsymbol{K}_p\boldsymbol{R}(\psi)^{\top}\tilde{\boldsymbol{\eta}} - \boldsymbol{K}_d\tilde{\boldsymbol{\nu}}, \tag{6b}$$

where $\tilde{\boldsymbol{\eta}} = \hat{\boldsymbol{\eta}} - \boldsymbol{\eta}_d$ and $\tilde{\boldsymbol{\nu}} = \hat{\boldsymbol{\nu}} - \boldsymbol{\nu}_d$ are the position and velocity error vectors, $\boldsymbol{\eta}_d$ and $\boldsymbol{\nu}_d$ are the desired position and velocity vectors from the reference system, $\boldsymbol{K}_p$, $\boldsymbol{K}_i$, and $\boldsymbol{K}_d \in \mathbb{R}^{3\times3}$ are diagonal non-negative PID controller gain matrices (see Fossen (2011) for more details). The states $\hat{\boldsymbol{\eta}}$ and $\hat{\boldsymbol{\nu}}$ are later replaced by the estimated states $\hat{\boldsymbol{\eta}}_m$ and $\hat{\boldsymbol{\nu}}_m$ from an observer.

2.4 Problem statement

Regardless of the environmental loads and thruster forces, the moored vessel becomes stable at the equilibrium point with only restoring forces from mooring lines. When each mooring line is equipped with a tension cell, the tension forces are measured. By this, we can estimate the relative position to the equilibrium point based on the tension measurements.

3 Design of the tension-based position reference system

We regard the moored vessel and all the anchors in the same horizontal plane. Assume all anchors are fixed anchor points and the vessel is a mobile unit in a sensor network. Then, we can estimate the position of the moored vessel through range-based localization techniques.

3.1 Mooring tension approximation

Regarding a specific catenary mooring line, the tension aroused from gravity performs as a restoring force to the moored vessel. Due to complexity of the catenary equations, the solution mainly calculate through the iterative approach. Therefore, a hypothetical mapping is given. The basic assumption for the algorithm is that the tension force at its upper end exists a mapping relation to the horizontal projected distance between the anchor and the upper end when $z = 0$, such that

$$T_i^0 = f_{X_i}(X_i) + \Delta T_{i,c} + \Delta T_{i,v}, \tag{7a}$$

$$T_i = T_i^0 + v_i, \quad i \in \mathcal{I}, \tag{7b}$$

where T_i^0 and T_i are the noiseless and noisy axial tension at the top end of the i^{th} mooring line, f_{X_i} is the mapping function, X_i is the distance between the i^{th} anchor and its fairlead, $\Delta T_{i,c}$ and $\Delta T_{i,v}$ are the tension variance due to current and heave motion. In this paper, it is assumed that $\Delta T_{i,c} = 0$. The nonzero current-introduced bias will be studied in future researches. Additionally, $\Delta T_{i,v}$ and v_i are supposed to be bounded zero-mean Gaussian white noise process. Based on the iteration results, f_{X_i} is a strictly continuously monotonic function. Therefore, its inverse function $f_{X_i}^{-1}(\cdot)$ exists.

3.2 Influence of the fairleads

Normally, the influence from the fairleads cannot be disregarded. We first assume the friction between the turret and the vessel is not remarkable. The turret can rotate with the restoring force. Additionally, the magnitude of the turret radius is much smaller than the lengths of the mooring lines. The arrangement is represented in Fig. 3. Since the angle $\Delta\theta$ is a small angle, we assume the COT is located in the extension line to the corresponding anchor and the fairlead with a certain distance r_t to the fairlead. Disregard the sea floor friction and the heave motion, such that $z = 0$, the mathematical expression is given by

$$d_i = f_{X_i}^{-1}(T_i) + r_t, \quad i \in \mathcal{I}, \tag{8}$$

where d_i is the projected horizontal distance between the i^{th} anchor and the COT. Obviously, d_i herein contains noise. We employ a passive observer in section 3.4 to filter the noise.

3.3 Preliminary position estimation

A group of M parallel estimators are constructed. The i^{th} estimator is based on the tension measurement T_j, where j belongs to an index set $\mathcal{J}_i := \mathcal{I}/\{i\} = [j_1^i, j_2^i, \ldots, j_N^i]$, $i \in \mathcal{I}$, and $N = M - 1$. This group scheme is applied to isolate the tension sensor fault from the GPS fault. Specifically, it needs only one estimator in the cases without fault tolerant control, such that $\mathcal{J} = \mathcal{I}$ and $N = M$.

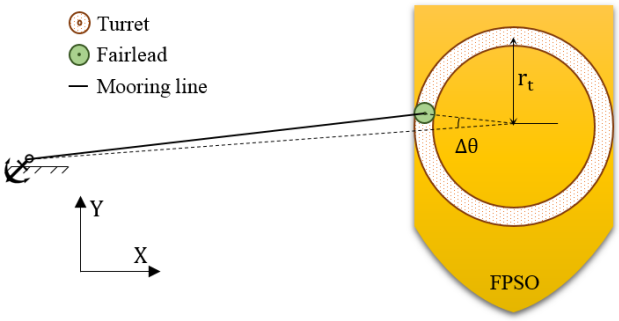

Fig. 3. The fairlead arrangement.

After knowing the distances between the COT and the anchor points, lateration can be utilized to locate the vessel. The triangular relation is given by

$$d_j^2 = (\hat{x} - x_j^a)^2 + (\hat{y} - y_j^a)^2, \quad i \in \mathcal{I}, \quad j \in \mathcal{J}_i, \tag{9}$$

where $[x_j^a, y_j^a]^\top$ is the position of the j^{th} anchor. There are N equations. Now we subtract the N^{th} equation from the first to the $(N-1)^{th}$ equations and write the result in a vector form,

$$\boldsymbol{A}_i \hat{\boldsymbol{p}}_i = \boldsymbol{b}_i, \quad i \in \mathcal{I}, \tag{10}$$

where

$$\boldsymbol{A}_i = \begin{bmatrix} 2(x_{j_1^i}^a - x_{j_N^i}^a) & 2(y_{j_1^i}^a - y_{j_N^i}^a) \\ 2(x_{j_2^i}^a - x_{j_N^i}^a) & 2(y_{j_2^i}^a - y_{j_N^i}^a) \\ \cdots & \cdots \\ 2(x_{j_{N-1}^i}^a - x_{j_N^i}^a) & 2(y_{j_{N-1}^i}^a - y_{j_N^i}^a) \end{bmatrix}, \tag{11}$$

and

$$\boldsymbol{b}_i = \begin{bmatrix} {x_{j_1^i}^a}^2 + {y_{j_1^i}^a}^2 - {x_{j_N^i}^a}^2 - {y_{j_N^i}^a}^2 - d_{j_1^i}^2 + d_{j_N^i}^2 \\ {x_{j_1^i}^a}^2 + {y_{j_1^i}^a}^2 - {x_{j_N^i}^a}^2 - {y_{j_N^i}^a}^2 - d_{j_2^i}^2 + d_{j_N^i}^2 \\ \cdots \\ {x_{j_{N-1}^i}^a}^2 + {y_{j_{N-1}^i}^a}^2 - {x_{j_N^i}^a}^2 - {y_{j_N^i}^a}^2 - d_{j_{N-1}^i}^2 + d_{j_N^i}^2 \end{bmatrix}, \tag{12}$$

Using the Moore-Penrose pseudo-inverse, we get the least-squares solution of the i^{th} estimator, that is

$$\hat{\boldsymbol{p}}_i = \boldsymbol{W}_i^{-1} \boldsymbol{A}_i^\top (\boldsymbol{A}_i \boldsymbol{W}_i^{-1} \boldsymbol{A}_i^\top)^{-1} \boldsymbol{b}_i, \tag{13}$$

where $\boldsymbol{W}_i$ is a positive weighted matrix (Fossen, 2011). When all the signals are equally weighted, e.g. $\boldsymbol{W}_i = \boldsymbol{I}$, (13) is simplified as

$$\hat{\boldsymbol{p}}_i = \boldsymbol{A}_i^\top (\boldsymbol{A}_i \boldsymbol{A}_i^\top)^{-1} \boldsymbol{b}_i. \tag{14}$$

The overall solution is the mean value of the solutions from all estimators, which is given by

$$\hat{\boldsymbol{p}} = \sum_{i \in \mathcal{I}} \hat{\boldsymbol{p}}_i / M. \tag{15}$$

3.4 Observer design

We include a nonlinear passive observer (NPO) to filter the noise caused by the heave motion and measurement noise, eliminate the wave-induced motion, and estimate unmeasured states from position estimation. The passive observers is introduced in the late 1990s by Fossen and Strand (1999). The main motivation was to overcome the difficulty of tuning numerous parameters in designing a Kalman filter. The NPO admits the realization

$$\dot{\hat{\boldsymbol{\eta}}}_{w,m} = \boldsymbol{A}_{\boldsymbol{pw}}(\omega_0) \hat{\boldsymbol{\eta}}_{w,m} + \boldsymbol{K_1} \tilde{\boldsymbol{y}}_m, \tag{16a}$$

$$\dot{\hat{\boldsymbol{\eta}}}_m = \boldsymbol{R}(\psi) \hat{\boldsymbol{\nu}}_m + \boldsymbol{K_2} \tilde{\boldsymbol{y}}_m, \tag{16b}$$

$$\dot{\hat{\boldsymbol{b}}}_m = -\boldsymbol{T}_b^{-1}\hat{\boldsymbol{b}}_m + \boldsymbol{K_3}\tilde{\boldsymbol{y}}_m, \tag{16c}$$

$$\begin{aligned} \boldsymbol{M}\dot{\hat{\boldsymbol{\nu}}}_m = &- \boldsymbol{D}\hat{\boldsymbol{\nu}}_m + \boldsymbol{R}(\psi)^\top \hat{\boldsymbol{b}}_m + \boldsymbol{\tau}_c \\ &+ \boldsymbol{R}(\psi)^\top \boldsymbol{T}(\hat{\boldsymbol{\beta}})\boldsymbol{\tau}_H + \boldsymbol{K_4}\boldsymbol{R}(\psi)^\top \tilde{\boldsymbol{y}}_m, \end{aligned} \tag{16d}$$

$$\hat{\boldsymbol{y}}_m = \hat{\boldsymbol{\eta}}_m + \boldsymbol{C}_{pw}\hat{\boldsymbol{\eta}}_{w,m}, \tag{16e}$$

where $\boldsymbol{y}_m = [\hat{\boldsymbol{p}}^\top \psi]^\top$, $\tilde{\boldsymbol{y}}_m = \boldsymbol{y}_m - \hat{\boldsymbol{y}}_m$ is the estimate error between the measurement $\boldsymbol{y}$ and the estimation $\hat{\boldsymbol{y}}$. $\boldsymbol{K_1} \in \mathbb{R}^{6\times3}$, $\boldsymbol{K_2} \in \mathbb{R}^{3\times3}$, $\boldsymbol{K_3} \in \mathbb{R}^{3\times3}$, and $\boldsymbol{K_4} \in \mathbb{R}^{3\times3}$ are the observer gain matrices, respectively. The subscript m means that the signals are from tension measurements.

4 Case Study I. Localization from tension measurements

4.1 Overview

The simulations are conducted in Simulink® with the MSS toolbox (MSS, 2010). The mooring system dimension is listed in Table 1. A ship-shape floating production storage and offloading (FPSO) is chosen as the research object. The detailed parameters are shown in Table 2.

Table 1. Mooring line dimensions.

Principle Dimension	Values
Dens. of ambient water $\rho_w(kg/m^3)$	1025
Length of the cable $L_m(m)$	2250
Elastic modulus $E_m Pa(M/m^2)$	4.5757×10^{10}
Cable cross section area $A_m(m^2)$	0.005
Cable diameter $d_m(m)$	0.08
Max strain ε	0.005
Position of the anchors	
$[x_1^a, y_1^a, z_1^a](m)$	$[1950, 0, -1000]$
$[x_2^a, y_2^a, z_2^a](m)$	$[0, 1950, -1000]$
$[x_3^a, y_3^a, z_3^a](m)$	$[-1950, 0, -1000]$
$[x_4^a, y_4^a, z_4^a](m)$	$[0, -1950, -1000]$
$[x_5^a, y_5^a, z_5^a](m)$	$[1378.9, 1378.9, -1000]$
$[x_6^a, y_6^a, z_6^a](m)$	$[-1378.9, 1378.9, -1000]$
$[x_7^a, y_7^a, z_7^a](m)$	$[-1378.9, -1378.9, -1000]$
$[x_8^a, y_8^a, z_8^a](m)$	$[1378.9, 0, -1000]$

Table 2. Vessel main particulars.

Principle Dimension	Values
Vessel Type	FPSO
Length between perp. L_{pp}	200
Breadth B(m)	44
Draught T(m)	12
Mass M(kg)	1.004e+08
Center of gravity C_G	[0,0,11]
Trans. metacentric height $\overline{GM_T}(m)$	5500
Long. metacentric height $\overline{GM_L}(m)$	7.95
Density of cable $\rho_k(kg/m^3)$	251.4

Simulation I.1: The first simulation aims to test if the tension-based localization approach is applicable. Assume that there is no noise in the tension measurements. Then, the NPO is not necessary in simulation I.1. For the sake of simplicity, it is assumed that the FPSO can move in the horizontal plane without any control limits. An additional assumption is that the turret does not have heave motion.

Simulation I.2: There exists noise in the tension measurements during practical operations. Therefore, noisy signal is a crucial issue to be considered. Independent Gaussian white noises with various variances are added to the tension measurements. Keep all the other conditions the same as Simulation I.1. This simulation tests the influence of the variance of tension sensor noise.

Simulation I.3: In addition to Simulation I.2, the moored FPSO starts to move in 6DOF, which means the heave motion influences the axial tensions. To verify the NPO, we herein apply strongly noisy tension measurements. Moreover, a GPS fault is triggered at $t = 400s$. It aims to test the isolability of the GPS fault.

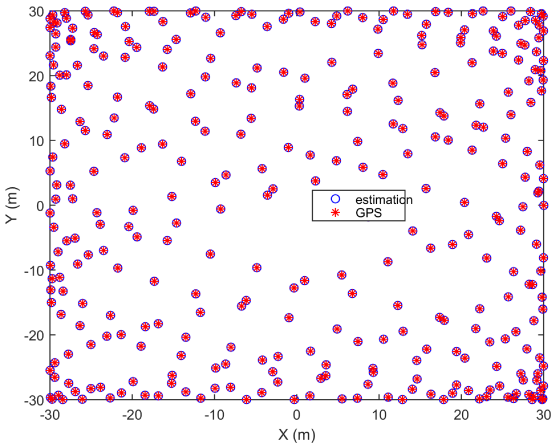

Fig. 4. Position estimate with no tension measurement noise.

4.2 Simulation results and discussion

4.2.1 Simulation I.1 From Fig. 4, we observe the tension-based estimation is quite close to the real GPS signals. From this simulation, the tension-based localization algorithm is applicable to provide position reference information to a moored vessel without noise and heave motion.

4.2.2 Simulation I.2 The overall simulation results are shown in Fig. 5, in which every point is the mean value of a group of results at 300 independent time instants. Mean square error (MSE) is employed as the criteria here to evaluate the localization performance, given by

$$MSE = |\boldsymbol{y}_m - \boldsymbol{y}|_2^2. \tag{17}$$

The smaller the criteria is, the better performance the estimator will have. The unit, dbm^2, comes from $10log_{10}(\cdot)$. We notice that the variance of localization is proportional to the variance of the tension measurement in the logarithmic coordinate. Hence, the smaller the variance of the tension measurements, the more precise positioning it can reach.

4.2.3 Simulation I.3 From Fig. 6, we notice that the error of $\boldsymbol{y}_m$ is bounded within a range. The estimation output from the NPO, $\hat{\boldsymbol{y}}_m$, has smaller errors. The errors between the tension-based position signals and the GPS signals are limited within $1.5m$. Therefore, the NPO gives good estimates of the vessel's position based merely on tension measurements. Additionally, the histograms shows that the estimation errors are approximately Gaussian distributed. The mean values of the estimation errors in x and z are about zero in the fault free condition. But the mean values in the faulty mode depend on the magnitude of fault. Therefore, the GPS failure is isolable.

5 Case Study II. Fault Diagnosis and Control Accommodation

5.1 Overview

The faulty measurement can be expressed as

$$\boldsymbol{y} = \boldsymbol{\eta} + \boldsymbol{L}_f \boldsymbol{y}_f(\tau), \tag{18}$$

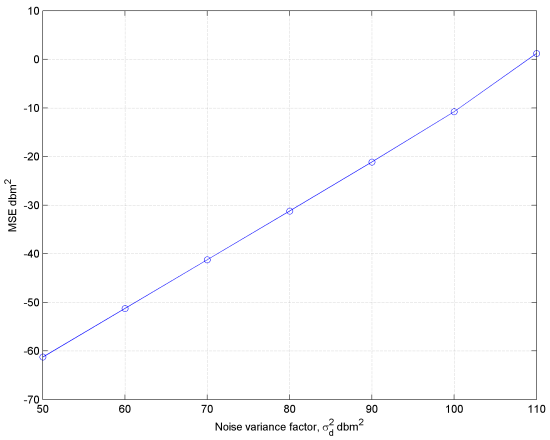

Fig. 5. A parameter analysis between the variance of the tension noise and the localization performance.

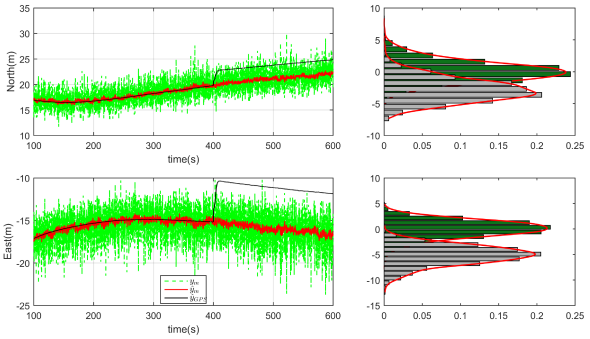

Fig. 6. Position estimation and the histograms of the residuals with tension measurement noise. The green bars are the error in the fault-free mode, and the gray bars are the results in the faulty condition.

where $\boldsymbol{L}_f = [\boldsymbol{I}_{2\times 2}\ \boldsymbol{0}_{2\times 1}]^\top$, and $\boldsymbol{y}_f(\tau) \in \mathbb{R}^2$ represents the GPS measurement faults in x and y direction, respectively. The fault is a bias that occurs in the period from t_{fs} to t_{ft},

$$\boldsymbol{y}_f(\tau) = \begin{cases} \boldsymbol{f} & \tau \in [t_{fs}, t_{ft}] \\ \boldsymbol{0} & else. \end{cases} \tag{19}$$

In this simulation, all the GPS signals are influenced due to the radio-wave absorption in upper medium frequency and lower high frequency ranges. Assume there are no additional faults occurring at the same time with the sensor fault. The design requirement is that the TAPM system can reconfigure the control inputs after the fault happens and recover after the fault disappears.

The TAPM system is exposed to ITTC spectrum waves and constant-velocity currents. The detailed environmental parameters are tabulated in Table 3. The GPS fault $\boldsymbol{f} = [10, 5]^\top$ (m) is triggered at $t_f = 2000$ seconds and ends at $t_f = 4000$ seconds.

5.2 Fault-tolerant control scheme

There are two types of faults, the GPS fault and the tension sensor faults. It is necessary to decouple the sensor fault from the GPS fault. Hereafter, we assume that single failure happens at one time instant. Based on the iteration

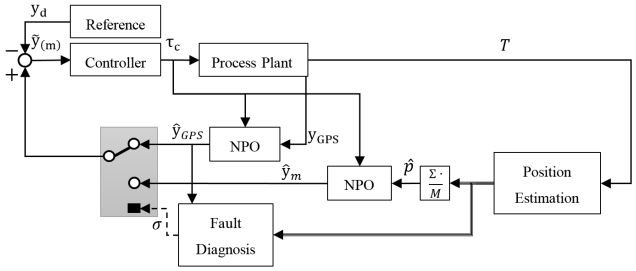

Fig. 7. The structure of the fault-tolerant controller.

results, we assume the bounded bias of a tension cell is not remarkable when comparing with the tension variance caused by the GPS drift, which has been verified in the Simulation I.3.

In the fault-free situation, the tension-based localization is more noisy than the GPS signal. The system is in closed-loop with the GPS signals and an open-loop tension-based localization algorithm. When the GPS failure happens, the tension-based localization approach can still relatively accurately estimate the position. But the GPS-based estimation no longer provides rational estimation. The scalar residual is the MSE of the GPS-based and the tension-based estimation, which is given by

$$r = |\hat{\boldsymbol{y}} - \hat{\boldsymbol{y}}_m|_2^2. \tag{20}$$

The estimated positions from the GPS and the tension-based posrefs are sent as inputs to a fault diagnosis module, which will detect the fault if the residual of the k^{th} estimator overpasses a specific accommodation upper threshold T_u. Then the k^{th} estimator set $\mathcal{J}_k$ is activated. Define a new set $\mathcal{K} \subseteq \mathcal{I}$, which represents a set contains all the indexes k of the activated $\mathcal{J}_k$. When the GPS fails, all estimators are unable to provide good estimations. The intersection of all activated estimator sets is an empty set. At this time, an alarm is required. When a failure exists in a tension sensor, all the estimators set are activated except the i^{th}. At this time, the intersection of all activated estimator set is $\{i\}$. Besides the above two conditions, a few tension cells may have poor measurements, caused by the biases in a few estimators. In such condition, the intersection of all the activated estimator set contains more than one member. Then, there is no alarm. Therefore, the isolation law is given by

$$\bigcap_{k\in\mathcal{K}} \mathcal{J}_k = \begin{cases} \{\emptyset\}, & \text{GPS failure,} \\ \{i\}, & i^{th} \text{ tension sensor fault,} \\ \text{others,} & \text{no faults.} \end{cases} \tag{21}$$

The controller can reconfigure to the GPS-fault mode based on the σ signal which is generated from the fault diagnosis module. It thereafter recovers based on the estimated states from the tension localization observer module. When the residual reduces to another specific lower threshold value T_l, the controller recovers to the GPS signal. Normally, $T_l \leq T_u$ to avoid unnecessary switches. In this simulation, we set $T_u = 8$(m) and $T_l = 4$(m).

Table 3. Environments distributions.

Environments Parameters	Symbol and Unit	Values
Current velocity	ν_c(m)	0.1
Current direction	β_c(deg)	0
Significant wave height	H_s(m)	5.5
Mean wave direction	β(deg)	45

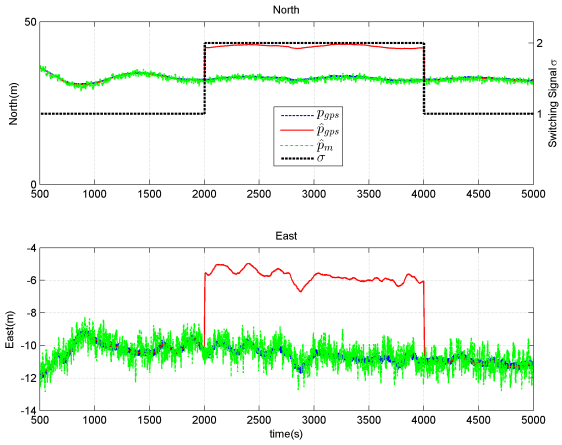

Fig. 8. NED position of the TAPM system with GPS fault happening in [2000,4000] seconds.

5.3 Simulation results and discussion

The simulation results are shown in Fig. 8. After the measurement fault on the GPS position happens, the controller quickly reconfigures the position information to tension-based localization estimates. The system is still stable. When the fault disappears at 4000 seconds, the controller recovers to the normal condition with the GPS measurements. The tension-based localization algorithm then has a more rapid oscillation than the GPS-based positions. However, the tension-based localization method provides reliable position signals after the fault happens, and the moored FPSO avoids a drive-off.

After the GPS fault happens, it takes four seconds to detect the faults. This delay is due to the integrator process in the observer, as well as the defensive logic in the diagnosis process. The reaction speed depends on the preset threshold values. Such delay also happens to the recovery process.

The simulation results prove the effectiveness of the proposed fault diagnosis strategy. The moored vessel remains in stable performance with only tension-based reference position.

6 Conclusion and Future Works

This paper deduced and verified a posref algorithm for TAPM systems depended on tension measurements. A fault-tolerant control scheme was illustrated based on this position algorithm. Future works includes range-based dynamic localization algorithm to handle parameter uncertainties, such as anchor positions, mooring line dynamics, sensor bias, and asynchronous signals. .

Acknowledgements

This work was supported by the Research Council of Norway (RCN) through the Centre for Research-based Innovation on Marine Operations (CRI MOVE), and the Centre of Excellence AMOS (RCN-project 223254). We thank Prof. Mogens Blanke for many discussions on fault-tolerant control. We would also like to acknowledge Dr. Bo Zhao for the discussion on applicable situations.

References

Aamo, O.M. and Fossen, T.I. (2001). Finite element modelling of moored vessels. *Mathematical and Computer Modelling of Dynamical Systems*, 7(1), 47–75.

Afraimovich, E.L., Kosogorov, E.A., and Leonovich, L.A. (2000). The use of the international gps network as the global detector (globdet) simultaneously observing sudden ionospheric disturbances. *Earth, planets and space*, 52(11), 1077–1082.

Blanke, M., Kinnaert, M., Lunze, J., and Staroswiecki, M. (2006). *Diagnosis and Fault-Tolerant Control, 2nd Edition*. Springer, Berlin, Heidelberg.

Doherty, P., Coster, A., and Murtagh, W. (2004). Space weather effects of octobernovember 2003. *GPS Solutions*, 8(4), 267–271.

Fang, S. and Blanke, M. (2011). Fault monitoring and fault recovery control for position-moored vessels. *International Journal of Applied Mathematics and Computer Science*, 21(3), 467–478.

Fang, S., Blanke, M., and Leira, B.J. (2015). Mooring system diagnosis and structural reliability control for position moored vessels. *Control engineering Practice*, 36, 12–26.

Fossen, T.I. (2011). *Handbook of marine craft hydrodynamics and motion control*. John Wiley & Sons.

Fossen, T.I. and Strand, J.P. (1999). Passive nonlinear observer design for ships using lyapunov methods: full-scale experiments with a supply vessel. *Automatica*, 35(1), 3–16.

Gauthier, S., Elletson, E., et al. (2014). Mooring line monitoring to reduce risk of line failure. In *The Twenty-fourth International Ocean and Polar Engineering Conference*. International Society of Offshore and Polar Engineers.

MSS. Marine Systems Simulator (2010). Viewed 30.10.2014. URL `http://www.marinecontrol.org`.

Nguyen, D.H., Nguyen, D.T., Quek, S.T., and Sørensen, A.J. (2011). Position-moored drilling vessel in level ice by control of riser end angles. *Cold Regions Science and Technology*, 66(2-3), 65–74.

Nguyen, D.T. and Blanke, M. (2015). Diagnosis and fault-tolerant positioning control for offshore vessels with thruster and mooring actuation. *International Journal of Adaptive Control and Signal Processing*, 00, 1–27.

Ren, Z., Skjetne, R., and Hassani, V. (2015). Supervisory control of line breakage for thruster-assisted position mooring system. In *10th IFAC Conference on Manoeuvring and Control of Marine Craft (MCMC2015)*. Copenhagen Denmark.

Skjetne, R., Imsland, L., and Lset, S. (2014). The Arctic DP Research Project: Effective Stationkeeping in Ice. *Modeling, Identification and Control*, 35(4), 191–210. doi:10.4173/mic.2014.4.1.

Sørensen, A.J. (2012). Marine control systems propulsion and motion control of ships and ocean structures lecture notes.

Tsugawa, T., Saito, A., Otsuka, Y., Nishioka, M., Maruyama, T., Kato, H., Nagatsuma, T., and Murata, K. (2011). Ionospheric disturbances detected by gps total electron content observation after the 2011 off the pacific coast of tohoku earthquake. *Earth, planets and space*, 63(7), 875–879.

Zhao, B., Blanke, M., and Skjetne, R. (2012). Particle filter rov navigation using hydroacoustic position and speed log measurements. In *American Control Conference (ACC), 2012*, 6209–6215.